High Efficiency Energy Extraction from a Relativistic Electron Beam in a Strongly Tapered Undulator

N. Sudar, P. Musumeci, J. Duris, and I. Gadjev
Particle Beam Physics Laboratory, Department of Physics and Astronomy, University of California Los Angeles, Los Angeles, California 90095, USA

M. Polyanskiy, I. Pogorelsky, M. Fedurin, C. Swinson, K. Kusche, and M. Babzien
Accelerator Test Facility, Brookhaven National Laboratory, Upton, New York 11973, USA

A. Gover
Faculty of Engineering, Department of Physical Electronics, Tel-Aviv University, Tel-Aviv 69978, Israel
(Received 3 May 2016; published 19 October 2016)

We present results of an experiment where, using a 200 GW CO_2 laser seed, a 65 MeV electron beam was decelerated down to 35 MeV in a 54-cm-long strongly tapered helical magnetic undulator, extracting over 30% of the initial electron beam energy to coherent radiation. These results, supported by simulations of the radiation field evolution, demonstrate unparalleled electro-optical conversion efficiencies for a relativistic beam in an undulator field and represent an important step in the development of high peak and average power coherent radiation sources.

DOI: 10.1103/PhysRevLett.117.174801

Greatly increasing the electro-optical conversion efficiency from particle beams to coherent radiation has the potential to enable a new class of high peak and average power sources capable of satisfying the increasing demands of cutting-edge scientific and industrial applications. These range from powering laser-based accelerators, developing high energy lasers for power beaming and laser propulsion, and improving the throughput of next generation fabrication processes for the semiconductor industry [1–4].

The current workhorse to directly convert power from electron beams to electromagnetic radiation is the free-electron laser (FEL) interaction where relativistic electron beams and electromagnetic waves exchange energy as they copropagate in an undulator magnetic field. This interaction is maximized when the electron energy, the undulator period, and field amplitude satisfy the resonant condition, or equivalently the particles slip exactly one (or an integer number of) radiation wavelength every undulator period. In the classical FEL scheme [5,6], the amplification process saturates at a peak power given by $P_{\mathrm{sat}} \sim 1.6\rho P_{\mathrm{beam}}$ where ρ is the FEL Pierce parameter (typically lower than 0.5% for short wavelength radiation) and P_{beam} is the beam power. Because of the absence of a gain medium or of a nearby metal or dielectric structure, the interaction is dissipation-free and saturation occurs only due to the fact that the particles lose energy and fall out of the resonant interaction region.

Increasing the output power beyond the FEL saturation level can be achieved by tapering the undulator parameters to sustain the interaction even when the particles lose a large fraction of their energy. Undulator tapering as a means to increase FEL performance has been studied since the early days of FEL technology when the FEL was proposed as a path towards very high average power sources, and typically results in few percent efficiencies. The ELF experiment in the 1980s demonstrated extraction efficiencies over 30% but for GHz frequencies and only in a waveguide-mediated interaction [7]. Recent development of the X-Ray FEL has rekindled interest in undulator tapering [8–10] as increase in the X-ray FEL peak power resulting from 5% to 10% extraction efficiencies could unlock long-term goals in x-ray science such as single molecule imaging [11,12].

An even stronger tapering of the undulator parameters to maintain the resonant condition over a very large (octave-spanning) beam energy variation has been studied in the context of inverse free electron laser (IFEL) accelerators [13–15]. For example, the Rubicon IFEL at the Accelerator Test Facility at the Broohaven National Laboratory recently demonstrated resonant acceleration of particles from an initial energy of 52 MeV to a final energy of ~95 MeV at a gradient of ~100 MeV/m, [16,17] using a 200 GW CO_2 laser pulse and a strongly tapered helical undulator.

In this Letter, we discuss the results of an experiment operating such an accelerator in reverse, that is, where the high power CO_2 laser and the tapered helical undulator are used to obtain high gradient deceleration, halving the final beam energy, showing unprecedented efficiency in energy extraction from a highly relativistic electron beam. In the experiment, named Nocibur or inverse Rubicon, a permanent magnet based prebuncher was also used to bunch the electrons and load them at the decelerating phase of the interaction to maximize trapping efficiency. In summary, a fraction larger than 45% of the injected 65 MeV beam was

 © 2016 American Physical Society

decelerated to ~35 MeV in the 54-cm-long tapered helical undulator using a 200 GW 10.3 μm laser pulse. These results, with the help of self-consistent simulations of the evolution of the radiation field, show for the first time the feasibility of reaching electro-optical energy conversion efficiencies as high as 30% in short wavelength laser-electron interactions [18–20].

The reverse tapering of the undulator was determined using the resonant phase and energy concepts first introduced in Kroll, Morton, and Rosenbluth [21]. The electrons traveling in the undulator gain or lose energy depending on their phase in the ponderomotive potential defined by the laser and undulator parameters. For helical geometry, the evolution of a particle energy is described by

$$\frac{d\gamma^2}{dz} = -2kK_lK\sin(\Psi) \tag{1}$$

where k and k_w are the laser and undulator wave numbers, $K_l = (eE_0/km_ec^2)$ and $K = (eB_0/k_wm_ec)$ are the laser and undulator vector potentials, and γ and Ψ represent the particle Lorentz factor and phase, respectively. We define a resonant energy such that a particle at γ_r will maintain a synchronous phase throughout the interaction, i.e.

$$\frac{d\Psi}{dz} = k_w - \frac{k(1+K^2)}{2\gamma^2} = 0 \rightarrow \gamma_r^2 = \frac{k(1+K^2)}{2k_w}. \tag{2}$$

To optimize the tapering (i.e. the variation of k_w and K along the undulator) we can derive a differential equation for the undulator parameters by equating the rate of change of the resonant energy [i.e. the derivative of Eq. (2)] with the ponderomotive gradient expression [Eq. (1)] for a resonant particle at a constant nonzero resonant phase, Ψ_r obtaining

$$\frac{dK}{dz} = \frac{(1+K^2)(dk_w/dz)}{2Kk_w} - k_wK_l\sin\Psi_r. \tag{3}$$

In our experiment, the resonant phase Ψ_r was set to $\pi/4$ as a compromise between the magnitude of the deceleration gradient and the extent of the stable region in longitudinal phase space where particles can be trapped and decelerated. Further, the variation of the period which defines (dk_w/dz) was predetermined by already existing undulator body and magnets. The Nocibur experiment in fact reutilized the Rubicon helical undulator made up of two $N_w = 11$ period Halbach undulators, oriented perpendicularly and shifted in phase by $\pi/2$ with period decreasing from 5.97 cm to 4.04 cm [see Fig. 1(a)]. The undulator field amplitude was then adjusted to match the new field profile obtained as a solution of Eq. (3) by varying the gap between the permanent magnets. Using the new undulator parameters, the resonant energy for 10.3 μm laser wavelength decreases

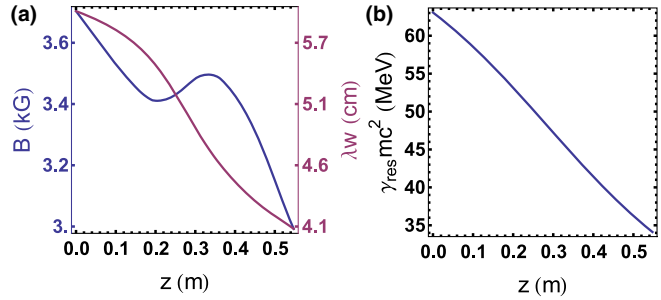

FIG. 1. Undulator period and magnetic field amplitude (left) and resonant energy (right) vs the coordinate z along the undulator axis.

from 65 MeV to 35 MeV along the interaction as shown in Fig. 1(b).

In order to inject as many particles as possible in the stable region of the ponderomotive potential and maximize the energy extraction efficiency, we utilized a modulator-chicane compact prebuncher. A single 5 cm period planar Halbach-style undulator is used as an energy modulator to impart a nearly 3% peak-to-peak energy modulation on the beam. Additional half period long sections at the entrance and exit of the undulator are used to correct for the trajectory offset. The modulator is immediately followed by a chicane composed of four dipole magnets of length 12.5 mm whose gap can be adjusted from a minimum of 13 mm to a maximum of 18 mm and are interspaced by drifts of 12.5 mm. The variable gap allows us to control the dispersion of the chicane and tune the transport matrix element R_{56} from 21 to 59 μm to obtain maximum bunching.

Figure 2 shows a schematic of the layout of the beam line with the prebuncher and undulator. A dipole is used to coalign the electron beam to the propagation axis of the CO_2 laser which is focused by a 4.5 m focal length NaCl lens (not shown) to a 0.99 mm waist in the middle of the undulator. Quadrupole magnets are used to focus the electron beam through the interaction and then transport it to the energy spectrometer. Experimental electron beam and laser parameters are listed in Table I. Picosecond scale timing between the laser and electron beam is achieved first by utilizing electron-beam controlled CO_2 transmission in a

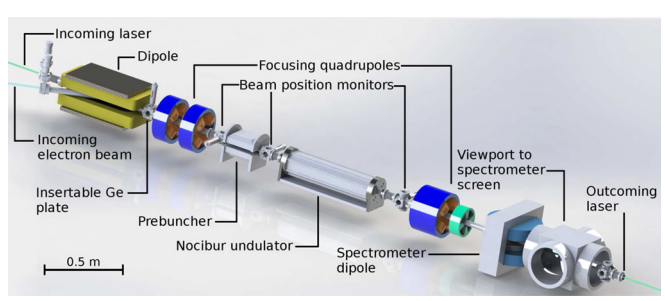

FIG. 2. Nocibur experiment beam line layout.

TABLE I. Parameters for the Nocibur experiment.

Parameter	Value
Initial electron beam energy	65 MeV
Initial beam energy spread ($(\Delta E/E)$)	0.0015
Electron beam emittance ($\epsilon_{x,y}$)	2 mm-mrad
Electron beam waist ($\sigma_{x,y}$)	100 μm
Electron beam current	100 A
Electron beam charge	100 pC
Laser wavelength	10.3 μm
Rayleigh range	0.3 m
Laser waist	990 μm
Laser waist position	$(L_u/2) = 0.275$ m
Laser M^2	1.1
Laser energy	0.3–0.7 J
Laser pulse length	3 ps

semiconductor (Ge) slab [22] and then adjusted by maximizing the energy modulation on the electron spectrometer.

Fine-tuning of the prebuncher-chicane gap is used to control the relative injection phase between the laser and the electron microbunches at the undulator entrance [Fig. 4(a)]. Studying the fraction of the particles captured as a function of the gap, we observe a peak of maximum trapping where the electron beam is delayed by $\sim(7\pi/4)\lambda$, corresponding to a slippage of the beam to the design resonant phase by $\pi/4$, Fig. 4(b).

In Fig. 3 we show two representative energy spectrometer images and the relative energy distribution projections $(1/N_{\rm tot})(dN/dE)$ normalized so that the integral under the curves is 1. The peak capture fraction was measured at ~45% for a 100 pC electron beam, injected at 65 MeV and decelerated down to 35 MeV, matching very well with the design simulations. By integrating over the energy distributions we can calculate the total energy in the electron beam, i.e., $E_{\rm tot} = (Q/e)\int[(1/N_{\rm tot})(dN/dE)EdE])$. When the drive laser is turned off, the electron beam is nearly monochromatic and $E_{\rm tot}$ is given by 100 pC $\times$ 65 MV $=$ 6.5 mJ. Averaging $E_{\rm tot}$ over the shots with the seed laser on, we obtain 4.5 ± 0.4 mJ, yielding an energy extraction efficiency of ~30%.

The full interaction was simulated with a general particle tracer (GPT) [23] using field maps from the 3D magnetostatic solver Radia[24], which agree well with the undulator and prebuncher Hall probe measurements. Simulations of the radiation produced in the undulator were carried out using the 3D time-dependent FEL simulation code GENESIS [25]. Figures 4(c) and 4(d) show the e-beam longitudinal phase space after the prebuncher as well as the final spectrum. Without prebunching, simulations indicate that the fraction of particles trapped by the IFEL decelerator would drop to 17%, reducing the extraction efficiency by nearly a factor of 3 to ~10%.

The output electron energy spectra from the experiment, GPT, and GENESIS are in excellent agreement validating the

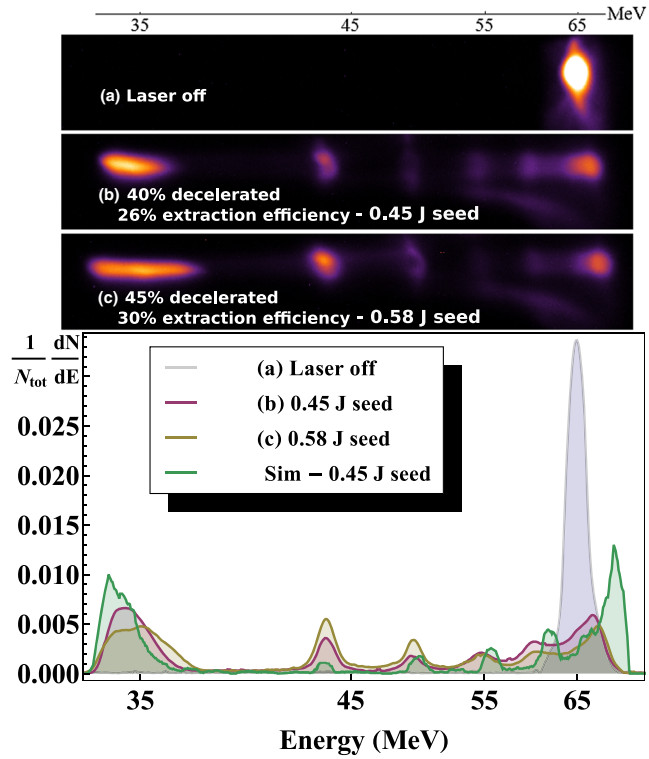

FIG. 3. (a) Electron beam spectrum with no laser seed. (b),(c) Deceleration spectra from Nocibur spectrometer for two consecutive shots having slightly different input laser seed energy, compared with GPT simulation $(1/N)(dN/dE)$ vs E (bottom).

assumption that minimal electromagnetic field evolution occurs along the interaction, Fig. 5(a). Genesis predicts an increase in radiation energy of 2 mJ consistent with the total energy lost by the electron beam. By comparing the simulated transverse profiles of the seed pulse with the output pulse [Fig. 5(b)] one notes that the newborn radiation comes out with a larger divergence angle, which should be expected since it is emitted by an electron beam focused to a much smaller spot size than the seed laser. Detection of the generated radiation was hindered by the presence of the large signal from the drive laser pulse.

The amplitude of the radiation field plays a crucial role in maximizing the energy extraction efficiency, and it is important to highlight the difference between coherent undulator radiation and stimulated superradiant emission. This can be understood by considering the field generated by the passage of a bunched beam in an undulator magnet, E_g, emitted coherently with a high power seed field, E_s. The superposition of the two fields yields a total radiation pulse energy, $\varepsilon \propto (\vec{E}_s + \vec{E}_g)^2 = |E_s|^2 + 2\Re[\vec{E}_s \cdot \vec{E}_g^*] + |E_g|^2$. The electromagnetic energy gained at the end of the undulator is then proportional to $\Delta\varepsilon \propto 2\eta_p E_s E_g \cos\phi + |E_g|^2$ where η_p is the polarization matching factor (usually unity if the laser is properly circularly polarized) and ϕ is the phase of the bunching current relative to the laser beam

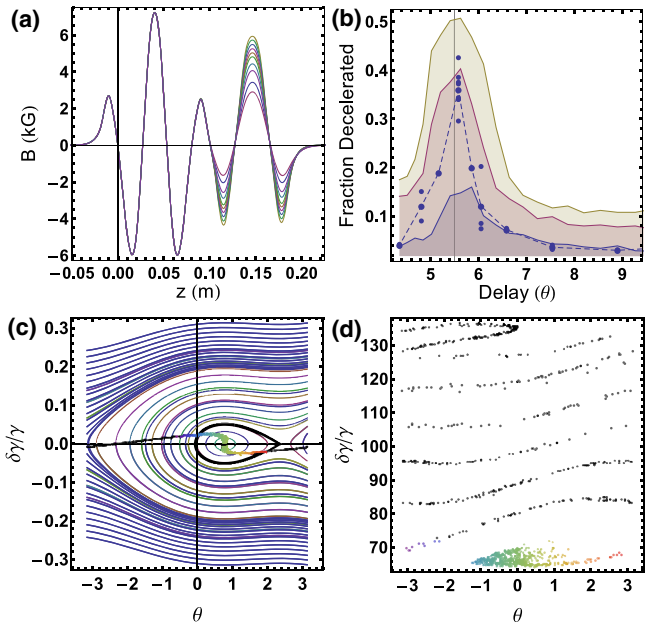

FIG. 4. (a) Hall probe measurements of the prebuncher field varying chicane gap. (b) Fraction of fully decelerated particles as a function of the injection phase controlled by varying the chicane gap compared with GPT simulations with seed energy 0.55 J (yellow), 0.45 J (red), and 0.35 J (blue). (c) Longitudinal phase space for $\Psi_r = \pi/4$ IFEL ponderomotive potential with phase space curves for trapped and untrapped particles. The prebunched beam longitudinal phase space is also shown color coding the particles within the separatrix. (d) GPT simulation of the e-beam spectrum at Nocibur exit showing full deceleration for the prebunched particles.

$(\cos\phi = \sin\psi_r = 1/\sqrt{2})$. The second term in this expression is the usual coherent undulator radiation. The first term represents the stimulated superradiant emission and for a large enough initial seed field can be dominating [26]. For example, in our case, if we calculate the coherent undulator emission from a perfectly microbunched 100 pC electron beam going through 11 undulator periods, we obtain 15 μJ. Both experiment and simulations show instead mJ-level energy exchange between the particles and the radiation as a result of the stimulated interaction.

An interesting feature of both experimental and simulation data is the discrete peaks in the energy spectrum. Much attention has been devoted in the literature to the motion of trapped particles, but an interesting effect is uncovered here for those electrons that follow open trajectories in phase space [27]. Looking at Fig. 4(c) it is observed that for the particular resonant phase $\pi/4$ these trajectories "bunch up" in energy at discrete levels. These energy levels can be calculated by finding the energy offsets for particles that have slipped ahead of the ponderomotive bucket by $2\pi n$. Using the Hamiltonian defined in [21], one can consider a detrapped particle, initially at $\delta\gamma = 0$, and calculate the energy deviation after its phase slips by 2π yielding $\delta\gamma(z) \sim \sqrt{\gamma_r(z)(d\gamma/dz)\lambda_w(z)}$. The

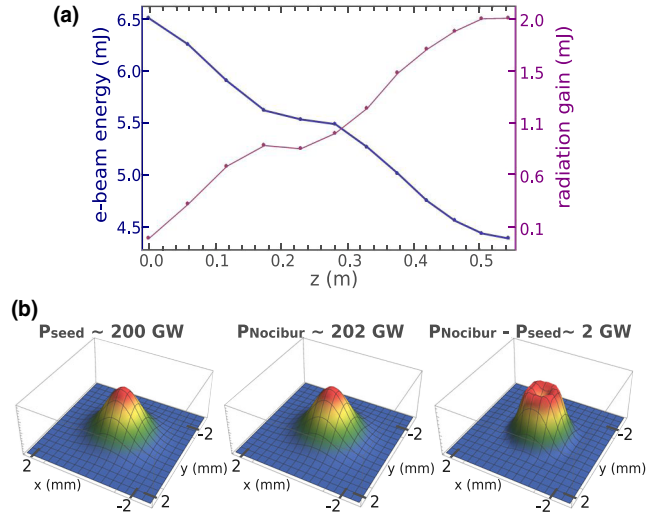

FIG. 5. (a) Evolution of the radiation energy gain and total energy in electron beam along the undulator from GENESIS simulation. (b) Transverse shape of Nocibur generated radiation at undulator exit.

positions for the energy peaks at larger $\delta\gamma$ can be solved for numerically using the full Hamiltonian. In Fig. 6 we show representative trajectories for the particles along the undulator from the GPT simulation in remarkable agreement with our estimates for the energy peaks using the Hamiltonian model. In principle, nonresonant IFEL interaction could find application in electron beam longitudinal phase space manipulation, for example, to stretch and reduce the energy spread of a microbunched beam injected in a tapered undulator just outside the trapping bucket.

In conclusion, the results from the Nocibur experiment show 30% electro-optical conversion efficiency from a

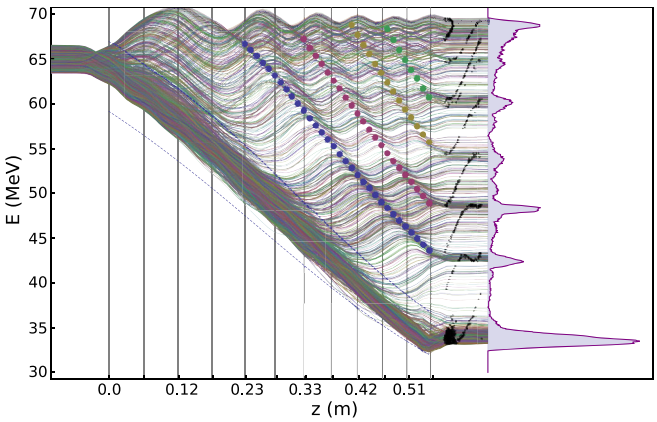

FIG. 6. Particle trajectories along the undulator from the GPT simulations. The (θ, γ) longitudinal phase space at the undulator exit from Genesis simulation is displayed to show the remarkable agreement in all details of the energy spectrum. The ponderomotive potential bucket height is represented by dashed lines. The estimates for the positions of the detrapped energy peaks are also shown (points).

relativistic electron beam setting a new record for an interaction occurring between a free-space propagating laser pulse and a relativistic electron beam, largely improving over early attempts to demonstrate high efficiency lasing in the far infrared regime [28]. This is mostly due to the developments in the generation of high brightness electron beams and increased seed laser quality and stability. It should be noted that Nocibur took advantage of the existing hardware and setup from an ongoing IFEL accelerator experiment and so was not optimized for radiation generation resulting in emitted power significantly lower than the input seed. Nevertheless the experiment shows that large improvements in efficiency can be obtained when prebunched beams, high intensity seed, and strongly tapered undulators are used, demonstrating for the first time the tapering-enhanced stimulated superradiant emission regime where the radiated energy is orders of magnitude larger than coherent emission.

The results show the path to reach similar efficiency at even shorter wavelengths where currently high average power coherent sources do not exist. In this case one may conceive an oscillator (or regenerative amplifier) configuration whereas the amplifier is embedded in an optical cavity with a large steady state circulating power optimized for high efficiency extraction with the tapered wiggler. The resonator round trip is tuned to be commensurate with the electron beam repetition rate. In such a scheme the electron beam only has to provide energy gain sufficient to overcome the cavity losses. To start up the oscillation, a high intensity short wavelength pulsed laser could be used as an igniter seed pulse. This is a subject for a separate study, but the present work stands as a proof of principle, showing that very high efficiencies are possible, thus opening the way towards new sources of very high power coherent radiation.

This work was partially supported by DOE Grant No. DE-SC0009914, U.S. DHS DNDO under Contract No. 2014-DN-077-ARI084-01, and by the U.S.-Israel Binational Science Foundation (BSF) Jerusalem, Israel. The authors would also like to thank Gerard Andonian and Ariel Nause for useful comments.

[1] E. Esarey, C. B. Schroeder, and W. Leemans, Rev. Mod. Phys. **81**, 1229 (2009).
[2] H. Bennett, Nucl. Instrum. Methods Phys. Res., Sect. A **341**, 124 (1994).
[3] K. J. Kim, A. A. Zholents, M. Zolotorev, and N. Vinourov, Nucl. Instrum. Methods Phys. Res., Sect. A **407**, 380 (1998).
[4] G. Dattoli *et al.*, Nucl. Instrum. Methods Phys. Res., Sect. A **474**, 259 (2001).
[5] J. M. J. Madey, H. A. Schwettman, and W. M. Fairbank, IEEE Trans. Nucl. Sci. **20**, 980 (1973).
[6] R. Bonifacio, C. Pellegrini, and L. M. Narducci, Opt. Commun. **50**, 373 (1984).
[7] T. J. Orzechowski *et al.*, Phys. Rev. Lett. **57**, 2172 (1986).
[8] W. M. Fawley, Z. Huang, K.-J. Kim, and N. A. Vinokurov, Nucl. Instrum. Methods Phys. Res., Sect. A **483**, 537 (2002).
[9] Y. Jiao, J. Wu, Y. Cai, A. W. Chao, W. M. Fawley, J. Frisch, Z. Huang, H.-D. Nuhn, C. Pellegrini, and S. Reiche, Phys. Rev. ST Accel. Beams **15**, 050704 (2012).
[10] C. Emma, K. Fang, J. Wu, and C. Pellegrini, Phys. Rev. ST Accel. Beams **19**, 020705 (2016).
[11] H. Chapman *et al.*, Nat. Phys. **2**, 839 (2006).
[12] S. Hau-Riege *et al.*, Phys. Rev. Lett. **98**, 145502 (2007).
[13] R. B. Palmer, J. Appl. Phys. **43**, 3014 (1972).
[14] E. D. Courant, C. Pellegrini, and W. Zakowicz, Phys. Rev. A **32**, 2813 (1985).
[15] J. T. Moody, S. G. Anderson, G. Anderson, S. Betts, S. Fisher, A. Tremaine, and P. Musumeci, Phys. Rev. Accel. Beams **19**, 021305 (2016).
[16] J. P. Duris *et al.*, Nat. Commun. **5**, 4928 (2014).
[17] J. P. Duris, Brookhaven National Laboratory's Accelerator Test Facility Report No. AE41 (2015).
[18] J. P. Duris, A. Murokh, and P. Musumeci, New J. Phys. **17**, 063036 (2015).
[19] A. Gover, Phys. Rev. ST Accel. Beams **8**, 030701 (2005).
[20] J. Duris, A. Murokh, and P. Musumeci, Tapering enhanced stimulated superradiant amplification, International Patent No. WO/2015/164531 (29 October 2015).
[21] N. M. Kroll, P. L. Morton, and M. N. Rosenbluth, IEEE J. Quantum Electron. **17**, 1436 (1981).
[22] D. B. Cesar, P. Musumeci, and D. Alesini, J. Appl. Phys. **118**, 234506 (2015).
[23] General Particle Tracer, http://www.pulsar.nl/gpt/.
[24] RADIA, http://www.esrf.eu/Accelerators/Groups/InsertionDevices/Software/Radia.
[25] S Reiche, P Musumeci, and K. Goldammer, *Proceedings of PAC 2007* (JACOW, 2007) P. 1269.
[26] A. Gover, R. Ianconescu, A. Friedman, C. Emma, and P. Musumeci, *Proceedings of FEL2015*, Daejeon, Korea (2015), WEP085, http://accelconf.web.cern.ch/AccelConf/FEL2015/papers/proceed.pdf.
[27] C. Behrens *et al.*, Nat. Commun. **5**, 3762 (2014).
[28] J. T. Weir *et al.*, Proc. SPIE Int. Soc. Opt. Eng. **97**, 1133 (1988).